# Scrutiny of human lung infection by SARS-CoV-2 and associated human immune responses in humanized mice

Zheng Hu[1,#], Renren Sun[1,#], Zongzheng Zhao[3,#], Cong Fu[1], Yixin Wang[1,4], Zhendong Chunmao Zhang[3], Lina Liu[8], Cheng Zhang[5], Chang Shu[1], Jin He[1], Wei Li[2,6], Qi Zhou[2,6,*], Yuwei Gao[3,*], Shucheng Hua[1,4,*], Yong-Guang Yang[1,7,*]

[1] Key Laboratory of Organ Regeneration & Transplantation of Ministry of Education, and National-Local Joint Engineering Laboratory of Animal Models for Human Diseases, The First Hospital of Jilin University, Changchun 130062, China

[2] State Key Laboratory of Stem Cell and Reproductive Biology, Institute of Zoology, Chinese Academy of Sciences, Beijing 100101, China

[3] Changchun Veterinary Research Institute, Chinese Academy of Agricultural Sciences, Changchun 130122, China

[4] Department of Respiration, The First Hospital of Jilin University, Changchun 130061, China

[5] College of Veterinary Medicine, Hebei Agricultural University, Baoding 071001, China

[6] Institute for Stem Cell and Regeneration, Chinese Academy of Sciences, Beijing 100101, China

[7] International Center of Future Science, Jilin University, Changchun 130012, China

[8] College of Veterinary Medicine, Jilin University, Changchun 130061, China

Running Head: Humanized mouse model of COVID-19

[#] These authors contributed equally to this work.

[*]Address correspondence to: yongg@jlu.edu.cn (Y.-G.Y.); shuchenghua@126.com

(S-C.H.); gaoyuwei@gmail.com (Y-W. G.); zhouqi@ioz.ac.cn (Q.Z.).

## ABSTRACT

There is an urgent need for animal models of COVID-19 to study immunopathogenesis and test therapeutic intervenes. In this study we showed that NSG mice engrafted with human lung (HL) tissue (NSG-L) could be infected efficiently by SARS-CoV-2, and that live virus capable of infecting Vero cells was found in the HL grafts and multiple organs from infected NSG-L mice. RNA-seq examination identified a series of differentially expressed genes, which are enriched in viral defense responses, chemotaxis, interferon stimulation, and pulmonary fibrosis between HL grafts from infected and control NSG-L mice. Furthermore, when infecting humanized mice with human immune system (HIS) and autologous HL grafts (HISL mice), the mice had bodyweight loss and hemorrhage and immune cell infiltration in HL grafts, which were not observed in immunodeficient NSG-L mice, indicating the development of anti-viral immune responses in these mice. In support of this possibility, the infected HISL mice showed bodyweight recovery and lack of detectable live virus at the later time. These results demonstrate that NSG-L and HISL mice are susceptible to SARS-CoV-2 infection, offering a useful *in vivo* model for studying SARS-CoV-2 infection and the associated immune response and immunopathology, and testing anti-SARS-CoV-2 therapies.

## Introduction

The globe pandemic of coronavirus disease 2019 (COVID-19) caused by severe acute respiratory syndrome coronavirus 2 (SARS-CoV-2) infection has affected over two hundred million people and caused more than four million deaths worldwide since the end of 2019. The lack of animal models that can be easily used to model SARS-CoV-2 infection and pathogenesis in biosafety level 3/4 facilities is an important drawback factor impeding mechanistic understanding of COVID-19 pathogenesis and test new anti-viral therapies[1]. Although mice are the most popular and easily handleable animal model, conventional murine models are not suitable for COVID-19 studies because most SARS-CoV-2 strains cannot use murine angiotensin I converting enzyme 2 (ACE2) to invade mouse cells[2]. Although human ACE2 transgenic mice have been shown susceptible to SARS-CoV-2 infection[3,4], this model overlooks other proteins involved, such as transmembrane serine protease 2 (TMPRSS2) and CD147[5,6]. In addition, profound evolutionary divergences between mice and humans also compromise their value to faithfully replicate viral infection process and the associated disorders[7]. Non-human primates are genetically close to human and can be infected by SARS-CoV-2[8], however, their wide usage is intensively restrained due to their extreme high cost and the need for complicated operating procedures especially in biosafety level 3/4 facilities. Thus, there is an urgent need for novel animal models that are easy to handle and faithfully mimic human SARS-CoV-2 infection and the associated immune responses.

Immune surveillance plays crucial roles in the control of viral infection and the development of inflammatory syndromes, including pneumonia and cytokine storm in COVID-19 patients[9]. Previous studies of ours and other groups have shown that human immune system (HIS) mice made by co-transplantation of human fetal thymic tissue (under renal capsule) and $CD34^+$ fetal liver cells (FLCs, i.v.)[10,11] could mount antigen specific human T and antibody responses following immunization, viral infections or transplantation[12-14]. Here we sought to extend this model to explore COVID-19 immunopathogenesis by grafting HIS mice with human lung (HL) tissue that is autologous to the human immune system of the HIS mice. We found that the HIS mice with HL xenografts (referred to as HISL mice) could be infected by SARS-CoV-2 virus and develop anti-viral immune responses, offering a convenient and useful *in vivo* model for understanding COVID-19 pathogenesis and testing anti-SARS-CoV-2 interventions.

## Results

### Entry and replication of SARS-CoV-2 and associated transcriptome changes in HL xenografts in mice

We first determined whether human HL tissue grafted in NOD/SCID $IL2rg^{-/-}$ (NSG) mice can be infected by SARS-CoV-2. Briefly, NSG mice were implanted subcutaneously with HL tissue (referred to as NSG-L mice), and subjected to infection via intra-HL injection of SARS-CoV-2 or PBS (as controls) 6-8 weeks later. Immunohistochemistry (IHC)

examination confirmed human ACE2 protein expression throughout the HL xenografts (Fig. 1a). Real-time qPCR (RT-qPCR) analysis revealed that SARS-CoV-2 RNA was detected in HL and various mouse tissues including heart, liver, spleen, lung, kidney, brain and intestine at days 1and 3 following inoculation of $10^6$ $TCID_{50}$ SARS-CoV-2, but not in NSG mice receiving subcutaneous injection of a similar number of virus (Fig. 1b), demonstrating SARS-CoV-2 infection and expansion in HL xenografts. To confirm this observation, another cohort of NSG-L mice were intra-HL inoculated with SARS-CoV-2 or mock. Again, viral copies were detected in HL at days 3, 5, 8, 14 and 21 after infection (Fig. 1c). Importantly, 13 out of 14 HL homogenate samples (except one at day 21) harvested from SARS-CoV-2-infected NSG-L mice at days 3, 5, 8, 14, and 21 after infection retained the capability to re-infect Vero E6 cells *in vitro*, demonstrating the existence of live SARS-CoV-2 in HL xenografts (Fig. 1d). However, viral inoculation did not lead to significant bodyweight loss (Fig. 1e) or detectable pathological changes in HL grafts (Fig. 1f) or mouse tissues (Supplementary Fig. 1), likely due to the immunodeficiency of NSG-L mice. This is in line with previous reports that the complications in COVID-19 patients are largely attributable to immune responses driven by SARS-CoV-2 infection[15].

**RNA-seq analysis for HL xenografts after SARS-CoV-2 infection**

To further understand the insight into SARS-CoV-2 infection induced changes in HL cells, we analyzed the transcriptome by RNA-seq of HL samples from uninfected NSG-L mice

or infected NSG-L mice 5 and 21 days after SARS-CoV-2 inoculation. For day-5 HL grafts, a total of 4612 human genes were differentially expressed between two samples, of which 2129 genes were significantly upregulated and 2483 genes were downregulated ($|log2(FoldChange)| > 1 \ \& \ padj < 0.05$) in SARS-CoV-2-infected compared to uninfected HL grafts (Fig. 2a left). For day-21 HL grafts, a total of 6488 human genes were differentially expressed between the two samples, of which 3311 and 3177 genes were significantly upregulated and downregulated ($|log2(FoldChange)| > 1 \ \& \ padj < 0.05$), respectively in SARS-CoV-2-infected compared to uninfected HL grafts (Fig. 2a right). Many of these differentially expressed genes are associated with viral defense responses, including NLRC5, MICB, APOBEC3D, APOBEC3G, IFI6, ISG15, and IFITM3, which were markedly upregulated in infected HL grafts at days 5 and 21 compared to HL grafts from uninfected NSG-L mice (Fig. 2b). Notability, HL grafts from the infected NSG-L mice showed a great upregulation of viral infection-associated chemokines (e.g., CCL11 and CXCL6 at day 5, and CCL19, CXCL19, CXCL13, CCL18 at day 21; Fig. 2c) and interferon-stimulated genes (ISGs; e.g., IFIT1 and STAT1 at day 5, and ISG15, IFITM1 and IFI27 at day 21; Fig. 2d) compared to those from non-infected NSG-L mice. Furthermore, SARS-CoV-2 infection induced intensive upregulation of genes involved in pulmonary fibrosis at day 5 (e.g. CSF1, FASLG, NLRP1) and day 21 (e.g. IGF2, IL18, MMP9) in infected HL grafts (Fig. 2e), providing a mechanistic explanation for the reported development of lung fibrosis, a long-term and presumably irreversible complication of COVID-19 patients[16]. Together, these findings support the

use of NSG-L mice as a convenient and useful *in vivo* platform for modeling human lung infection with SARS-CoV-2 and testing anti-viral therapies.

**Development of antiviral immunity in HISL mice following SARS-CoV-2 infection**

We next examined SARS-CoV-2 infection in HISL mice with both HL and human immunity. Briefly, HISL mice were constructed by transplantation of HL and thymic tissues and $CD34^+$ cells, and subjected to SARS-CoV-2 infection after human immune reconstitution was confirmed by measuring human immune cells in peripheral blood. FACS analysis of PBMCs 14 weeks after humanization detected high levels of human $CD45^+$ lymphohematopoietic cells composed of $CD3^+$ T cells (including both CD4 and CD8 T cells), $CD20^+$ B cells and $CD33^+$ myeloid cells in HISL mice (Fig. 3a). Furthermore, human $CD45^+$ immune cells including $CD4^+$ T cells, $CD20^+$ B cells and $CD11c^+$ dendritic cells were also detected in spleen and HL grafts from these mice (Fig. 3b). These HISL mice were infected 3 weeks later with SARS-CoV-2 or mock as controls. Unlike NSG-L mice (Fig. 1), HISL mice showed a significant bodyweight loss after intra-HL SARS-CoV-2 infection, which returned to a level comparable to the control HISL mice by 21 days (Fig. 4a). No mortality was observed in HISL mice infected with SARS-CoV-2. Furthermore, HL grafts from HISL mice that received SARS-CoV-2 (but not mock) had hemorrhage at day 5, which was associated with increased infiltration by human $CD45^+$ cells, including $CD4^+$ T and $CD20^+$ B cells (Fig. 4b). Although the levels of human T and B cell infiltration in HL grafts became comparable between the two

groups at day 21, there were still significantly more human $CD33^+$ myeloid cells (Supplementary Fig. 2a), including $CD11c^+$ cells (Supplementary Fig. 2b), in HL grafts in SARS-CoV-2-infected than mock infected mice, which is in line with previous reports for patients[17,18]. No significant difference was detected for any human immune cell populations in WBCs, including $CD3^+$ T, $CD20^+$ B, $CD33^+$ myeloid, and $CD56^+$ NK cells between SARS-CoV-2- and mock-infected mice at day 21 (Supplementary Fig. 2c). Viral copies were detected by RT-qPCR in all HL samples (except one at day 21) from SARS-CoV-2-infected HISL mice, but not those from the control HISL mice (Fig. 4c). However, in contrast to HL homogenates from infected NSG-L mice (Fig. 1), HL homogenate samples from most infected HISL mice harvested at day 5 (5 out 6) and day 21 (5 out 6) failed to infect Vero E6 cells *in vitro* (Fig. 4d), indicating an efficient elimination of live SARS-CoV-2 by human immune system in these mice.

## Discussion

Mouse models are considered more convenient than non-human primates for *in vivo* studies on infectious diseases that are required to be performed in biosafety level 3/4 facilities. Lack of cross reaction between rodent ACE2 and the coronavirus protein S prevents effective invasion of SARS-CoV-2 in mice. To overcome this obstacle, mice with transgenic expression of human ACE2 were recently created and demonstrated to be susceptible to SARS-CoV-2 infection[3,4]. However, human ACE2-trangenic mice do not express other proteins, such as TMPRSS2 and CD147, which are potentially involved in

SARS-CoV-2 infection[5,6]. In this study, we explored SARS-CoV-2 infection in NSG-L and HISL mice. The NSG-L model was created by a simple procedure of HL subcutaneous implantation in NSG mice. We confirmed that the HL grafts in these mice remained lung histology and ACE2 expression and were susceptible to SARS-CoV-2 infection. Furthermore, live virus capable of infecting Vero E6 cells was detected in HL grafts and multiple organs from NSG-L mice infected with SARS-CoV-2, indicating an efficient SARS-CoV-2 replication in these mice. These results demonstrate that NSG-L mice, which can be easily constructed and comfortably used in ABSL-3 laboratories, offer an effective *in vivo* model for identifying and comparing different viral strains and testing the efficacy of anti-viral drugs including neutralizing antibodies (Fig. 5).

HISL mice were constructed by transplantation of HL and thymic tissues and $CD34^+$ cells. The HISL mice not only carried HL grafts, but also human immune system that is autologous to the HL, hence these mice developed anti-viral immune responses and complications associated with immunopathogenesis following SARS-CoV-2 infection. Although not capable of modeling upper respiratory or systemic infection/manifestations, as only the HL xenograft is susceptible to SARS-CoV-2 in these mice, this model is still useful as the only currently available model that permits *in vivo* assessment of human immune responses against SARS-CoV-2 infection. Therefore, HISL mice are a convenient and useful *in vivo* platform for evaluating the immunopathology of COVID-19 and the efficacy of anti-viral immunotherapies, such as vaccination (Fig. 5).

Respiratory viral entry and propagation in lung parenchymal cells induce native viral defense responses and associated changes in inflammatory regulating gene expression[19]. Dynamic transcriptome alternations in human lung parenchymal cells after SARS-CoV-2 infection remain largely unknown. In this study, we found that there were large numbers of differentially expressed genes between HL grafts from SARS-CoV-2-infected and control NSG-L mice, which were enriched for anti-viral defense responses, and the associated chemokines and interferon stimulated genes. We also identified a marked upregulation of genes involved in pulmonary fibrosis, providing an explanation for lung fibrosis found in COVID-19 patients[16]. These data support the use of NSG-L mice as an *in vivo* model to study the kinetic changes in gene expression profiles caused by interaction between SARS-CoV-2 and human lung parenchymal cells.

Immune surveillance not only play a crucial role in viral clearance but is also involved in the immunopathogenesis and complications following viral infection. Unlike the immunodeficient NSG-L mice, SARS-CoV-2 infection in HISL mice induced significant bodyweight loss and HL tissue hemorrhage and inflammatory cell infiltration, demonstrating the development of anti-viral immune responses in these mice. The effectiveness of these anti-vital responses in HISL mice was further confirmed by the absence of live virus by 5 days and bodyweight recovery at a later time. This suggests that the clinical symptoms were caused mainly by inflammation/immune responses, but

not viral invasion directly, supporting the use of HISL mice to study COVID-19 pathogenesis and anti-SARS-CoV-2 immunotherapy.

## References


1 Munoz-Fontela, C. *et al.* Animal models for COVID-19. *Nature* **586**, 509-515 (2020).

2 Wang, Q. *et al.* Structural and functional basis of SARS-CoV-2 entry by using Human ACE2. *Cell* **181**, 894-904 e899 (2020).

3 Bao, L. *et al.* The pathogenicity of SARS-CoV-2 in hACE2 transgenic mice. *Nature* **583**, 830-833 (2020).

4 Zheng, J. *et al.* COVID-19 treatments and pathogenesis including anosmia in K18-hACE2 mice. *Nature* **589**, 603-607 (2021).

5 Qiao, J. *et al.* The expression of SARS-CoV-2 receptor ACE2 and CD147, and protease TMPRSS2 in human and mouse brain cells and mouse brain tissues. *Biochem Biophys Res Commun* **533**, 867-871 (2020).

6 Wang, K. *et al.* CD147-spike protein is a novel route for SARS-CoV-2 infection to host cells. *Signal Transduct Target Ther* **5**, 1-10 (2020).

7 Perrin, S. Preclinical research: Make mouse studies work. *Nature News* **507**, 423 (2014).

8 Blair, R. V. *et al.* Acute respiratory distress in aged, SARS-CoV-2-infected african green monkeys but not rhesus macaques. *Am J Pathol*, **191**, 274-282 (2021).

9 Sariol, A. *et al.*. Lessons for COVID-19 immunity from other coronavirus infections. *Immunity* **53**, 248-263 (2020).

10 Lan, P. *et al.* Induction of human T-cell tolerance to porcine xenoantigens through mixed hematopoietic chimerism. *Blood* **103**, 3964-3969 (2004).

11 Lan, P. *et al.* Reconstitution of a functional human immune system in immunodeficient mice through combined human fetal thymus/liver and $CD34^+$ cell transplantation. *Blood* **108**, 487-492 (2006).

12 Tonomura, N. *et al.* Antigen-specific human T-cell responses and T cell-dependent production of human antibodies in a humanized mouse model. *Blood* **111**, 4293-4296 (2008).

13 Tonomura, N. *et al.* Pig islet xenograft rejection in a mouse model with an established human immune system. *Xenotransplantation* **15**, 129-135 (2008).

14 Brainard, D. M. *et al.* Induction of robust cellular and humoral virus-specific adaptive immune responses in human immunodeficiency virus-infected humanized BLT mice. *J Virol* **83**, 7305-7321 (2009).

15 Vardhana, S. A. *et al.* The many faces of the anti-COVID immune response. *J Exp Med* **217**, 6 (2020).

16 Grillo, F. *et al.* Lung fibrosis: an undervalued finding in COVID-19 pathological series. *Lancet Infect Dis* **21**, e72 (2020).

17 Szabo, P. A. *et al.* Longitudinal profiling of respiratory and systemic immune responses reveals myeloid cell-driven lung inflammation in severe COVID-19.

*Immunity* **54**, 4 (2021).

18 Nienhold, R. *et al.* Two distinct immunopathological profiles in autopsy lungs of COVID-19. *Nature Communications* **11**, 1-13 (2020).

19 Vabret, N. *et al.* Immunology of COVID-19: Current State of the Science. *Immunity* **52**, 910-941 (2020).

## Methods

**Mice and human tissues.** NOD-Prkd$^{cem26Cd52}$Il2rg$^{em26Cd22}$/Nju (referred to as NSG) mice were purchased from Nanjing Biomedical Research Institute of Nanjing University. All mice were housed in a specific pathogen-free (SPF) microisolator environment and used between 6-8 weeks of age. Discard human fetal samples of gestational age of 17-21 weeks were obtained with informed consent at the First Hospital of Jilin University. Human fetal thymic and lung tissues were cut into small pieces with a diameter of around 1 mm or 5 mm, respectively, and CD34$^+$ cells were purified from fetal liver cells (FLCs) by magnetic-activated cell sorting (MACS; with a purity of >90% confirmed by FACS). The human tissues and cells were cryopreserved in liquid nitrogen until use. Protocols involved in the use of human samples and animals were reviewed and approved by the Institutional Review Board and Institutional Animal Care and Use Committee of the First Hospital of Jilin University, and all experiments with SARS-CoV-2 (COVID-19) were performed in biosecurity level 3 laboratory according to the protocols approved by the Changchun Veterinary Research Institute, Chinese Academy of Agricultural Sciences.

**NSG-L mouse and HISL humanized mouse model construction.** NSG-L mice were

made by subcutaneous implantation of human fetal lung tissue (approximately 5 mm in diameter). HISL humanized mice were made by implantation of human fetal thymic tissue (around 1 mm in diameter; under the renal capsule) and lung tissue (5 mm in diameter; subcutaneously) in NSG mice that pre-conditioned with 1.75 Gy total body irradiation (TBI; Rad Source RS2000), followed by intravenous injection of 1-2$\times 10^5$ human $CD34^+$ FLCs (given 6-8 hours after TBI).

**Flow cytometric analysis.** Mouse PBMCs were prepared using density gradient centrifugation with Histopaque 1077 (Sigma-Aldrich, St. Louis, MO). Human immune cell reconstitution in humanized mice were determined by flow cytometry using following fluorochrome-conjugated antibodies: anti-human CD45, CD3, CD20, CD33, CD4, CD8; anti-mouse CD45 and Ter119 (BD Pharmingen). Examination was performed on a Cytek Aurora (Cytek Biosciences) and data were analyzed using the FlowJo software. Dead cells were excluded from the analysis by gating out propidium iodide retaining cells.

**SARS-CoV-2 virus preparation and titer determination.** SARS-CoV-2 (BetaCoV/Beijing/IME-BJ05-2020) was proliferated in Vero E6 cells, which are maintained in Dulbecco's modified Eagle's medium (DMEM; Invitrogen, Carlsbad, CA, USA) with supplemented 2% fetal bovine serum (FBS; Gibco, Auckland, New Zealand). Viral titers were determined using a standard 50% tissue culture infection dose ($TCID_{50}$) assay.

**Mouse experiments.** NSG-L or HISL mice were anesthetized with isoflurane and injected with 100 μl of $10^6$ $TCID_{50}$ of SARS-CoV-2 or PBS into the human lung (HL)

299 graft. The mice were followed for bodyweight changes, and euthanized for measuring
300 viral particles and histological changes in HL grafts and tissues at indicated time points.

301 **RNA extraction and RT-qPCR.** Total RNA was extracted from tissues homogenates
302 using the RNeasy Mini Kit (Qiagen, Hilden, Germany), and viral RNA loads were
303 determined by a SARS-CoV-2 RNA detection kit (Shenzhen Puruikang Biotech, China).
304 The viral RNA loads for the target SARS-CoV-2 N gene was normalized to the standard
305 curve obtained by using a plasmid containing the full-length cDNA of the SARS-CoV-2
306 N gene. The reactions were performed with CFX96 system (BIO-RAD, America)
307 according to the following protocol: 50 ℃ for 20 min for reverse transcription, followed
308 by 95 ℃ for 3 min and then 45 cycles of 95 ℃ for 5 s, 56 ℃ for 45 s. Results were
309 presented as log10 numbers of genome equivalent copies per gram of sample.

310 **Histology.** Tissues were embedded in paraffin, and sectioned (2.5 μm) for H&E and
311 immunohistochemistry (IHC) examination. For IHC, tissue sections were firstly stained
312 with monoclonal anti-human CD45 (DAKO, 2B11+PD7/26), CD20 (DAKO, L26), CD4
313 (ABclonal; ARC0328), or CD11c (Abcam; EP1347Y), ACE2 (Abcam; EPR4435(2))
314 antibodies, and the immunoreactivity was detected with UltraSensitiveTM
315 Streptavidin-Peroxidase Kit (KIT-9710, Mai Xin, China) according to the manufacturer's
316 protocol.

317 **RNA-seq.** Total RNA was polyA-selected, fragmented and the samples were examined
318 on an Illumina Novaseq6000 machine, yielding an average of 22 million uniquely aligned

paired-end 150-mer reads per sample. Reads were aligned with STAR RNA-seq aligner (Version 2.7.3a) using the UCSC/hg38 genome assembly and transcript annotation[20]. Expression levels were calculated as Fragments per Kilobase of transcript per Million reads (FPKM) using Cufflinks software[21]. Differential expression analysis was performed using Cuffdiff (version 2.2.1.Linux_x86_64)[21]. In each analysis, genes with thresholds of |log 2 (foldchange)| > 1, *p adj* < 0.05 and a mean FPKM value of more than 5 were tested. "Cluster Profiler" package (Release 3.16.1)[22] and "DOSE" package (Release 3.14.0 )[23] in R software (version 4.0.2) was used for functional enrichment analysis, and GO biological processes terms at the significant level (*q-value* < 0.05) were employed.

**Statistical analysis.** Data were analyzed using GraphPad Prism 8 software (San Diego, CA, USA) and presented as mean values ± SEM. The results were compared statistically using unpaired two-tailed Student's t test and two-way analysis of variance (ANOVA), and a p value of ≤ 0.05 was considered significant.

## Data availability

RNA-seq data have been deposited into the National Center for Biotechnology Information (NCBI) Gene Expression Omnibus (GEO) database under accession numbers GSE175900. The datasets generated during and/or analyzed during the current study are available from the corresponding author on reasonable request.

## References

20 Dobin, A. *et al.* STAR: ultrafast universal RNA-seq aligner. *Bioinformatics* **29**, 15-21 (2013).

21 Trapnell, C. *et al.* Transcript assembly and quantification by RNA-Seq reveals unannotated transcripts and isoform switching during cell differentiation. *Nat Biotechnol* **28**, 511-515 (2010).

22 Yu, G. *et al*. clusterProfiler: an R package for comparing biological themes among gene clusters. *OMICS* **16**, 284-287 (2012).

23 Yu, G. et al. DOSE: an R/Bioconductor package for disease ontology semantic and enrichment analysis. Bioinformatics 31, 608-609 (2015).

## Acknowledgements

This work was supported by grants from the Strategic Priority Research Program of the Chinese Academy of Sciences (XDA16030303), Chinese MOST (2017YFA0104402) and NSFC (91742107, 81870091, 91642208, 82001697 and 81941008), Science development project of Jilin province (20190201295JC and 20200703012ZP), and special grants for COVID-19 research of Jilin province (20200901006SF).

## Author contributions

Z.H., Q.Z., Y-W. G., S-C.H, Y-G.Y. conceived the study; Z.H., R-R.S., Z-Z.Z.,Y-X.W., C.S., J.H. performed the experiments; C.F. contributed to RNA-seq data analysis; Z.H., Q.Z., Y-W.G.,S-C.H. supervised the work; W.L. contributed to the discussion of the results; Z.H., R-R.S., Z-Z.Z., C.F. Y-G.Y. analyzed the data and wrote the manuscript; all authors edited and approved the manuscript..

## Competing interests

The authors declare that they have no competing financial interests.

366 **Figure legends**

367 **Fig.1 SARS-CoV-2 infection of HL xenografts in NSG mice.** NSG-L mice were
368 subjected to SARS-CoV-2 infection ($10^6$ $TCID_{50}$ given by intra-HL injection) 6-8 weeks
369 after HL transplantation. Data from two independent experiments are presented, in which
370 NSG mice receiving subcutaneous injection of SARS-CoV-2 (**b**) or NSG-L mice
371 receiving intra-HL injection of PBS (**c-f**) were used as controls, respectively. **a**,
372 Representative IHC images of HL xenografts (up, isotype; down, human ACE2). **b**, Viral
373 copies in the indicated tissues examined by RT-qPCR 1 (n=2 and 1 for HL-infected and
374 control groups, respectively) or 3 (n=1 per group) days after infection. **c-f**, Viral RNA
375 copies examined by RT-qPCR (**c**) and titers measured by Vero E6 cells (**d**) in HL
376 xenografts, and bodyweight changes (**e**) at the indicated time points (n=3 per group); **f**,
377 Representative H&E images of HL xenografts at day 5 after intra-HL injection of PBS
378 (left) or SARS-CoV-2 (right).

379

380 **Fig.2 RNA-seq analysis for HL grafts from NSG-L mice after SARS-CoV-2 infection.**
381 HL grafts injected with $10^6$ $TCID_{50}$ SARS-CoV-2 virus were harvested from NSG-L mice
382 for RNA-seq examination at day 5 and 21 after infection; Naïve HL graft without
383 infection was used as control. **a**, Volcano plot showing DEGs of HL grafts for
384 SARS-CoV2-infected at day 5 (left) or day 21 (right) and non-infection control from
385 NSG-L mice. The data for all genes are plotted as log2 fold change versus the −log10 of
386 the adjusted p-value. **b-e**, Heatmaps of RNA-seq expression Z-scores computed for

selected genes that are differentially expressed ($p\ adj < 0.05$, |log 2 (foldchange)| > 1) between 3 pairwise comparisons (L_E5 vs L_E21, Lung vs L_E5, Lung vs L_E21). **b**, DEGs under GO term "defense response to virus" (BP GO: 0051607); **c**, Chemokines; **d**, Interferon-stimulated genes; **e,** DEGs under DO term "Pulmonary Fibrosis" (DOID:3770).

**Fig.3 Human immune reconstruction in HISL mice.** HISL mice were made by co-transplantation of human fetal lung tissue (subcutaneous) together with autologous human fetal thymic tissue (under renal capsule) and $CD34^+$ FLCs in NSG mice and used for examination. **a**, Human immune cell chimerism in PBMCs of HISL mice at week 14. **b**, IHC images of spleen (up) and HL (down) sections of HISL mice stained for human CD45, CD4, CD20, and CD11c.

**Fig.4 HISL mice are susceptible for SARS-CoV-2.** HISL mice were infected at week 17 post-humanization with mock or $10^6$ $TCID_{50}$ SARS-CoV-2 into HL. **a**, Bodyweight changes of HISL mice infected with SARS-CoV-2 (n=6) or mock (n=4). **b**, Representative H&E and IHC images of HL sections of HISL mice infected with SARS-CoV-2 (n=6) or mock (n=4) at day 5. **c-d**, Mice were euthanized at days 2, 5, and 21 post-infection, and SARS-CoV-2 viral copies (**c**) and viral titers (**d**) in HL were examined (each symbol represents an individual animal). $*P < 0.05$.

**Fig.5 Schema of NSG-L and HISL mice and their potential use in COVID-19 studies.**

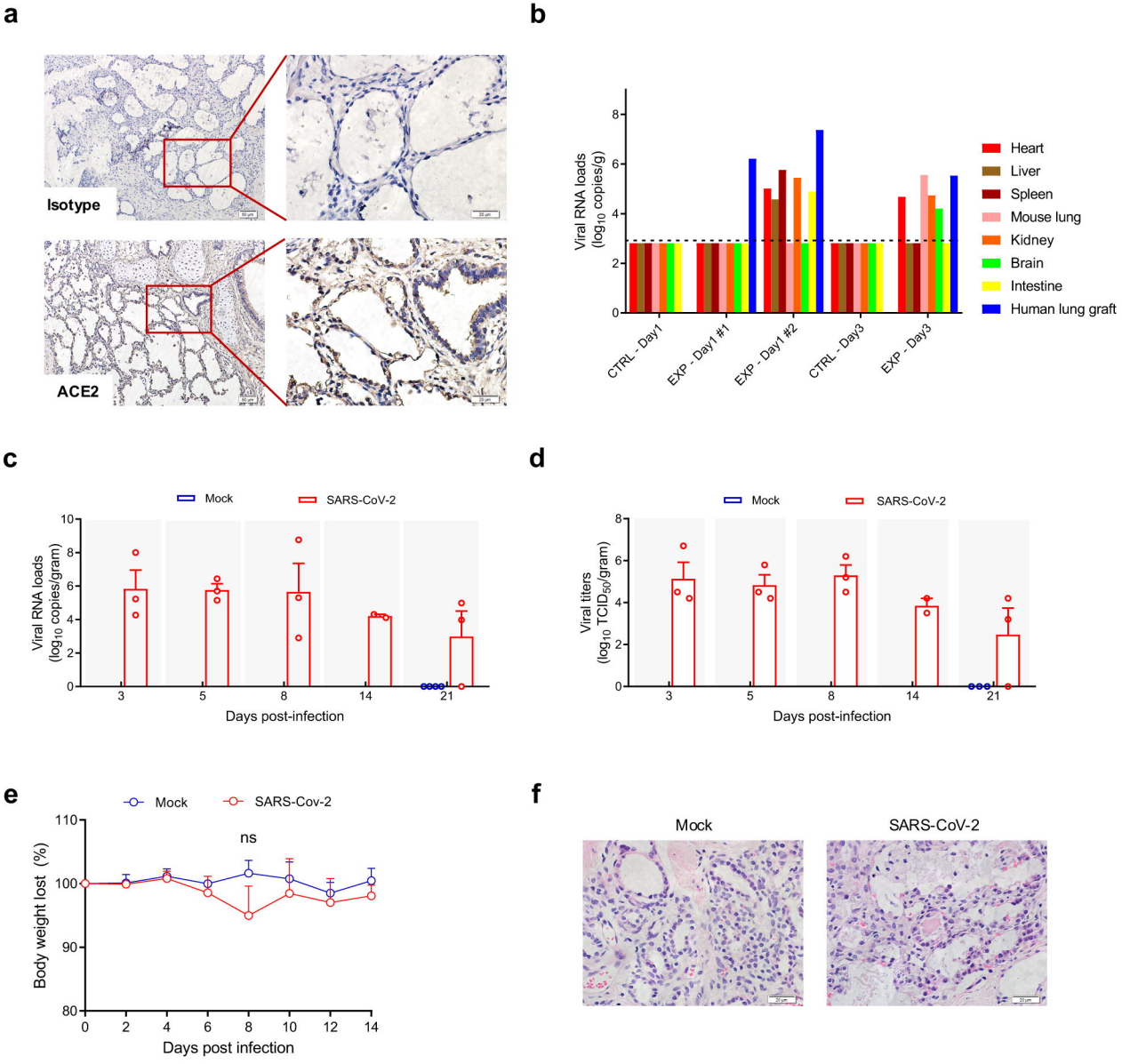
a
Isotype
ACE2
b
Viral RNA loads
(log10 copies/g)
Heart
Liver
Spleen
Mouse lung
Kidney
Brain
Intestine
Human lung graft
CTRL - Day1
EXP - Day1 #1
EXP - Day1 #2
CTRL - Day3
EXP - Day3
c
Mock
SARS-CoV-2
Viral RNA loads
(log10 copies/gram)
Days post-infection
d
Mock
SARS-CoV-2
Viral titers
(log10 TCID50/gram)
Days post-infection
e
Mock
SARS-Cov-2
ns
Body weight lost (%)
Days post infection
f
Mock
SARS-CoV-2

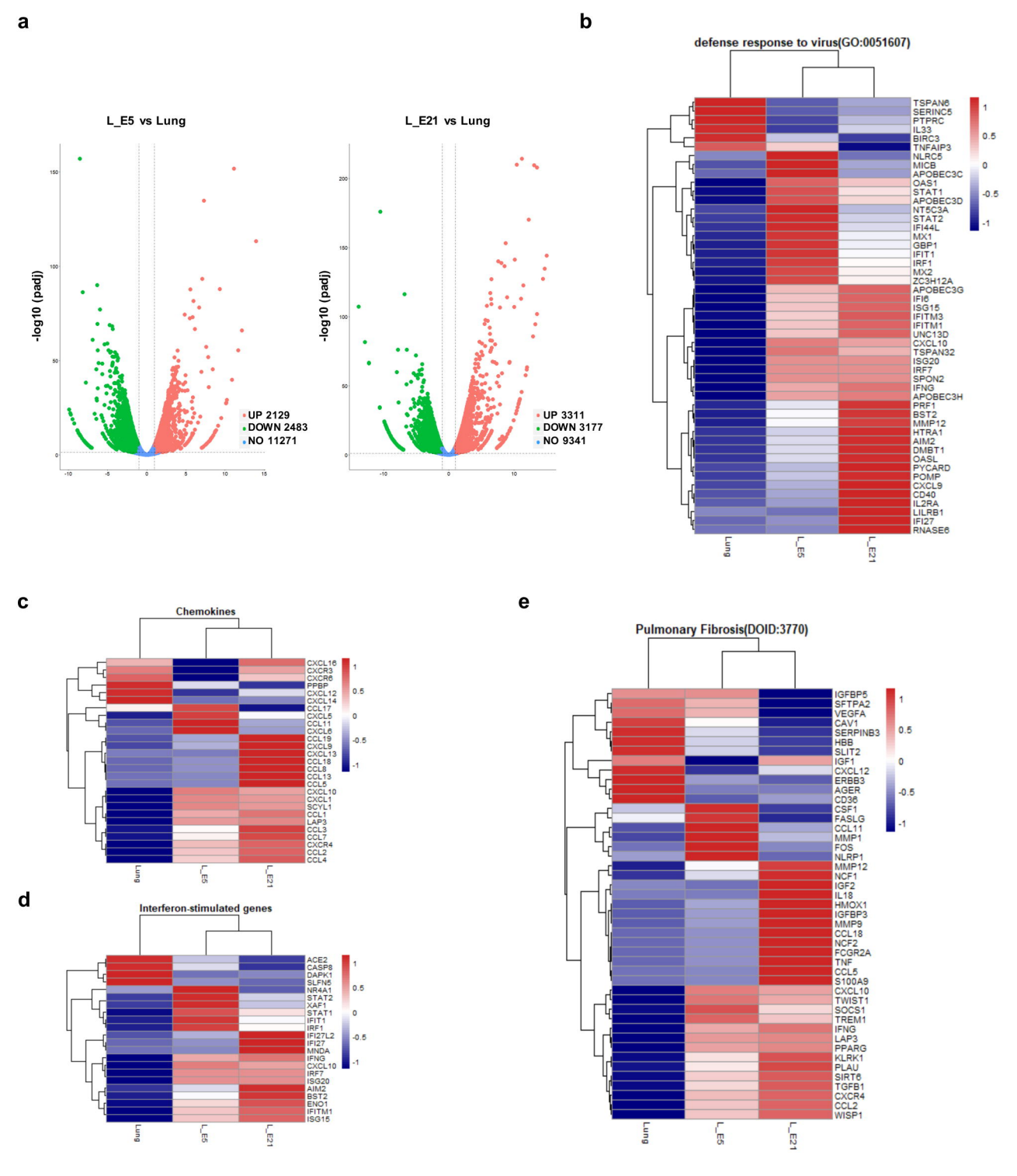
a
L_E5 vs Lung
-log10 (padj)
UP 2129
DOWN 2483
NO 11271
L_E21 vs Lung
-log10 (padj)
UP 3311
DOWN 3177
NO 9341
b
defense response to virus(GO:0051607)
TSPAN6
SERINC5
PTPRC
IL33
BIRC3
TNFAIP3
NLRC5
MICB
APOBEC3C
OAS1
STAT1
APOBEC3D
NT5C3A
STAT2
IFI44L
MX1
GBP1
IFIT1
IRF1
MX2
ZC3H12A
APOBEC3G
IFI6
ISG15
IFITM3
IFITM1
UNC13D
CXCL10
TSPAN32
ISG20
IRF7
SPON2
IFNG
APOBEC3H
PRF1
BST2
MMP12
HTRA1
AIM2
DMBT1
OASL
PYCARD
POMP
CXCL9
CD40
IL2RA
LILRB1
IFI27
RNASE6
Lung
L_E5
L_E21
c
Chemokines
CXCL16
CXCR3
CXCR6
PPBP
CXCL12
CXCL14
CCL17
CXCL5
CCL11
CXCL6
CCL19
CXCL9
CXCL13
CCL18
CCL8
CCL13
CCL5
CXCL10
CXCL1
SCYL1
CCL1
LAP3
CCL3
CCL7
CXCR4
CCL2
CCL4
Lung
L_E5
L_E21
d
Interferon-stimulated genes
ACE2
CASP8
DAPK1
SLFN5
NR4A1
STAT2
XAF1
STAT1
IFIT1
IRF1
IFI27L2
IFI27
MNDA
IFNG
CXCL10
IRF7
ISG20
AIM2
BST2
ENO1
IFITM1
ISG15
Lung
L_E5
L_E21
e
Pulmonary Fibrosis(DOID:3770)
IGFBP5
SFTPA2
VEGFA
CAV1
SERPINB3
HBB
SLIT2
IGF1
CXCL12
ERBB3
AGER
CD36
CSF1
FASLG
CCL11
MMP1
FOS
NLRP1
MMP12
NCF1
IGF2
IL18
HMOX1
IGFBP3
MMP9
CCL18
NCF2
FCGR2A
TNF
CCL5
S100A9
CXCL10
TWIST1
SOCS1
TREM1
IFNG
LAP3
PPARG
KLRK1
PLAU
SIRT6
TGFB1
CXCR4
CCL2
WISP1
Lung
L_E5
L_E21

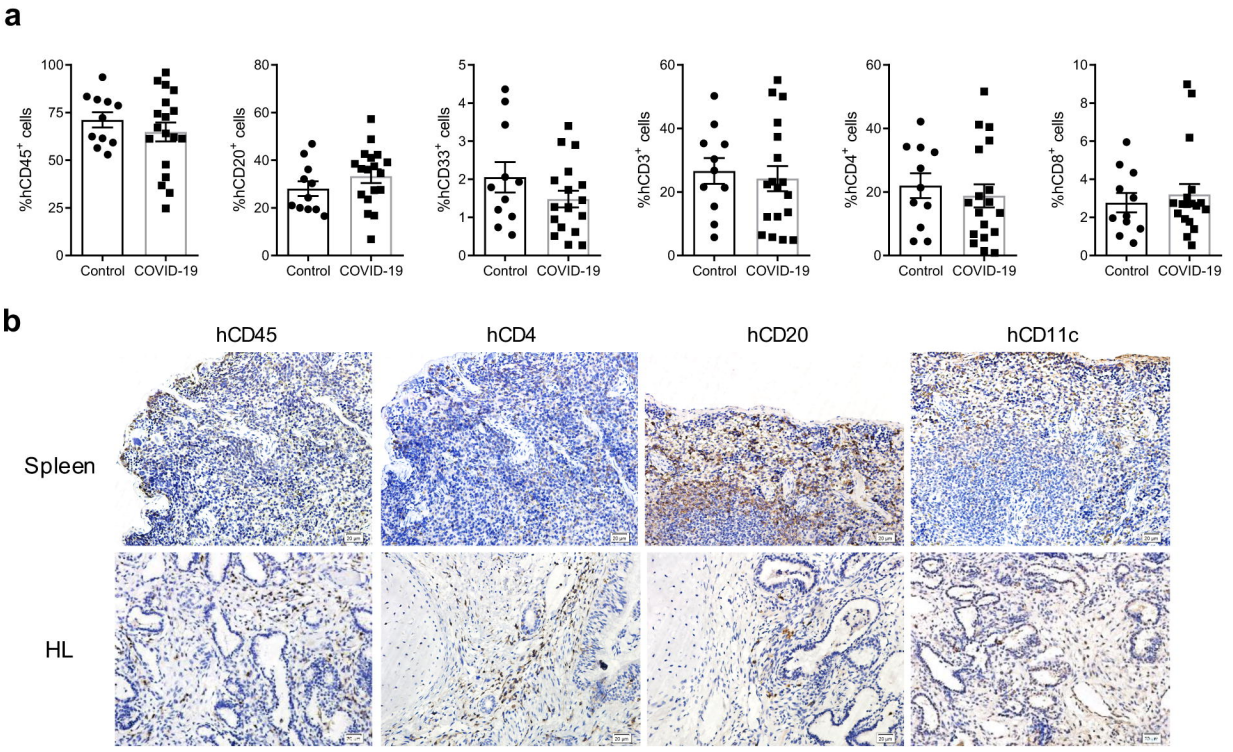
a
%hCD45+ cells
%hCD20+ cells
%hCD33+ cells
%hCD3+ cells
%hCD4+ cells
%hCD8+ cells
Control
COVID-19
b
hCD45
hCD4
hCD20
hCD11c
Spleen
HL

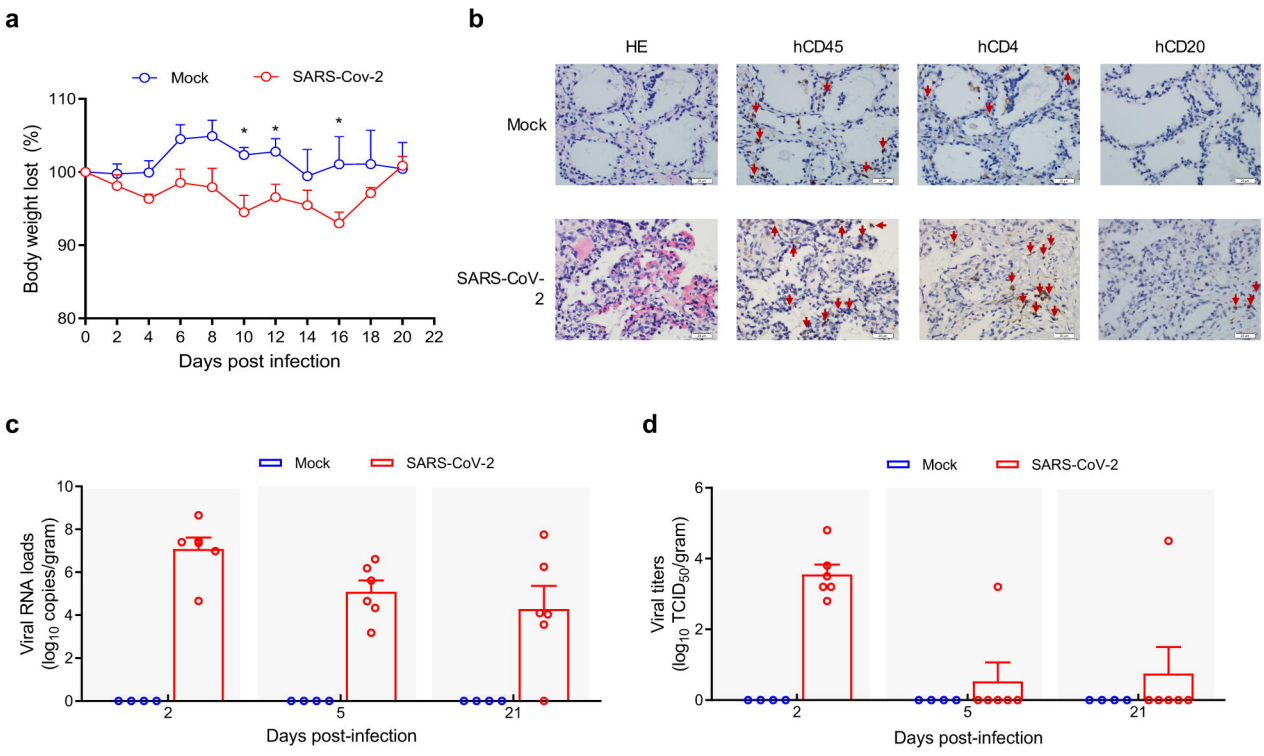
a
Mock
SARS-Cov-2
Body weight lost (%)
Days post infection
b
HE
hCD45
hCD4
hCD20
Mock
SARS-CoV-2
c
Mock
SARS-CoV-2
Viral RNA loads (log10 copies/gram)
Days post-infection
d
Mock
SARS-CoV-2
Viral titers (log10 TCID50/gram)
Days post-infection

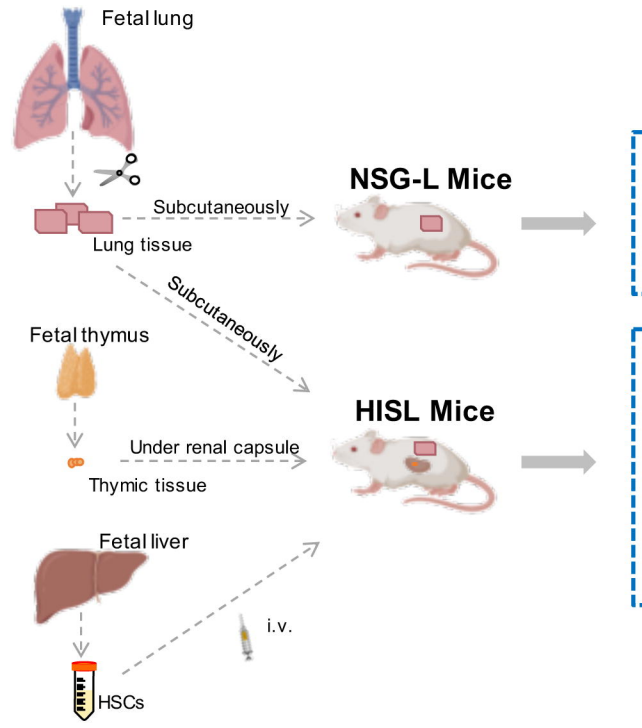


- Easily to prepare and use in ABSL-3 laboratories.
- Effective in identifying and comparing different viral strains and testing anti-viral drugs (e.g., neutralizing antibodies).

- Bearing both HL and human immune system, developing anti-SARS-CoV-2 immune responses.
- Permitting in vivo studies of human immune responses against SARS-CoV-2 infection
- A useful model for evaluating COVID-19 immunopathology and testing anti-viral immunotherapies (e.g., vaccines).